4774 J. Med. Chem. 2009, 52, 4774–4785
DOI: 10.1021/jm900371z

Journal of Medicinal Chemistry Article

Synthesis and Biological Evaluation of Guanidino Compounds Endowed with Subnanomolar Affinity as Competitive Inhibitors of Maize Polyamine Oxidase

Fabrizio Manetti,[†,§] Alessandra Cona,[‡,§] Lucilla Angeli,[†,§] Claudia Mugnaini,[†] Francesco Raffi,[†] Caterina Capone,[‡] Elena Dreassi,[†] Alessandra Tania Zizzari,[†] Alessandra Tisi,[‡] Rodolfo Federico,[‡] and Maurizio Botta*[,†]

[†]*Dipartimento Farmaco Chimico Tecnologico, Università degli Studi di Siena, Via Alcide de Gasperi 2, I-53100 Siena, Italy, and* [‡]*Dipartimento di Biologia, Università Roma Tre, Viale G. Marconi 446, I-00146 Roma, Italy.* [§] *These authors contributed equally to this work.*

Received March 24, 2009

Previous studies on agmatine and its derivatives suggested that the presence of hydrophobic groups on the guanidine moiety was a crucial key for inhibitory activity of maize polyamine oxidase. Accordingly, new lipophilic agmatine and iminoctadine derivatives were synthesized and tested for their ability to inhibit this enzyme. Several compounds showed an affinity in the nanomolar range, while a cyclopropylmethyl derivative of iminoctadine was found to be the most potent inhibitor of maize polyamine oxidase reported so far (K_i = 0.08 nM).

Introduction

Polyamine oxidases (PAOs[a]) are flavin adenine dinucleotide (FAD) dependent enzymes involved in the catabolism of ubiquitous polyamines via oxidative deamination of spermidine (Spd), spermine (Spm), and/or their acetylated derivatives at the secondary amino group.[1−3] PAOs represent a heterogeneous family of enzymes whose substrate specificity, kinetic properties, and mode of substrate oxidation vary depending on the biological source.[1−3] The chemical identity of the reaction products reflects the mode of oxidation of the substrate, which is alternatively cleaved at the carbon located on the endo-side or on the exo-side of the N4-nitrogen, giving rise to polyamine terminal catabolism (PAO from *Zea mays*,[4] *Hordeum vulgare*,[5] *Avena sativa*)[6] or back-conversion pathway (animal N^1-acetyl-PAO,[7] spermine oxidase,[8] yeast Fms1,[9] *Arabidopsis thaliana* PAO1,[10] *Arabidopsis thaliana* PAO3),[11] respectively. Aminoaldehydes and H_2O_2 are common products to both pathways of polyamine oxidation.

The great interest devoted to PAOs is derived from the physiological relevance of their substrates, which are essential growth factors, as well as from the cytotoxic properties of their reaction products, such as aminoaldehydes and H_2O_2. In this regard, both the modulation of polyamine homeostasis and the production of toxic compounds confer to PAO a crucial regulative role in cell proliferation and death in normal and cancer cells.

The search for selective inhibitors of polyamine biosynthesis enzymes started with the purpose to develop pharmacological strategies able to inhibit tumor growth.[1,12] Only recently, interest was turned on the polyamine catabolic pathway because of the attribution of programmed cell death (apoptosis) induction to the PAO-mediated H_2O_2 production in different tumor cell types.[13−15] Likewise, by means of both pharmacological and small interfering RNA strategies, it was demonstrated that spermine oxidase (SMO) mediated oxidative stress causes macrophage apoptosis in epithelial stomach cells infected by *Helicobacter pylori*[16] and can potentially contribute to gastric cancer development.[17] SMO expression and activity are induced by *H. pylori*, and inhibition of SMO activity with the inhibitor MDL 72527 (Chart 1) reduces both H_2O_2 production and apoptosis.[16] Since oxidative stress is potentially carcinogenic because of its ability to damage DNA, it was proposed that SMO-dependent H_2O_2 production represents a potential mechanism for inflammation-induced carcinogenesis.[17,18] Consistently, it was demonstrated that tumor necrosis factor-α (TNF-α), a proinflammatory cytokine, induces H_2O_2 production and oxidative DNA damage in epithelial cells through SMO-catalyzed spermine oxidation.[18] Analogously, the PAO-dependent H_2O_2 production in plants was shown to contribute to hypersensitive cell death occurring after pathogen attack.[19]

In addition, the neurotoxicity of reactive aldehydes, which are mediators of neurodegeneration in a number of neurological disorders such as Alzheimer's disease, is now well established. Particularly, 3-aminopropanal is an endogenous mediator of neuronal and glial cell death during cerebral ischemia.[20]

Zea mays PAO (ZmPAO, formerly MPAO) is the first PAO whose tertiary structure has been determined,[21,22] and over the past years it has become the reference enzyme as far as structure−activity relationships are concerned. Indeed, molecular modeling of mouse SMO,[23] *Hordeum vulgare* PAO1 (HvPAO1, formerly BPAO1), *Hordeum vulgare* PAO2 (HvPAO2, formerly BPAO2), and *Arabidopsis thaliana* PAO1 (AtPAO1)[5] revealed that the global fold of all the four proteins strictly resembles that of ZmPAO. Consistently, PAOs from different sources show similar affinity toward

*To whom correspondence should be addressed. Phone: +39 0577 234306. Fax: +39 0577 234333. E-mail: botta@unisi.it.

[a] Abbreviations: PAO, polyamine oxidase; Spd, spermidine; Spm, spermine; SMO, spermine oxidase; TNF, tumor necrosis factor; ZmPAO, *Zea mays* polyamine oxidase; HvPAO1 (formerly BPAO1), *Hordeum vulgare* polyamine oxidase-1; HvPAO2 (formerly BPAO2), *Hordeum vulgare* polyamine oxidase-2; AtPAO1, *Arabidopsis thaliana* polyamine oxidase-1; G3, *N*-prenylagmatine; APAO, animal N^1-acetylpolyamine oxidase; MD, molecular dynamics; GA, genetic algorithm.

 Published on Web 07/10/2009

Chart 1. Structures of Polyamine Inhibitors of PAO

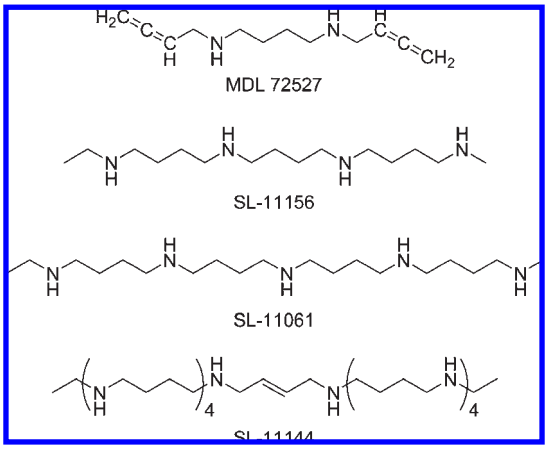

different ligands,[24] and therefore, ZmPAO protein represents an important model protein in designing new inhibitors suitable for every animal or plant PAOs.

The availability of selective and powerful PAO inhibitors would appreciably contribute to the study of polyamine homeostasis and to design new anticancer drugs. Inhibitors of PAO activity belong to four main classes: (i) linear primary diamines lacking secondary amino groups (such as 1,8-diaminooctane, **1**, Table 1)[25] and diamine derivatives;[26] (ii) agmatine (**2**) and its analogues, including *N*-prenylagmatine (G3, **3**),[27] compounds **4**−**9**,[28] and compounds **10**−**16**; (iii) diguanidino inhibitors, such as iminoctadine (**17**, a component of the guazatine mixture)[27] and its analogues (**18**−**24**), which represent the most powerful PAO inhibitors; (iv) polyamine analogues lacking terminal amino groups including the Spm analogue MDL 72527 (Chart 1)[26] and three new powerful PAO inhibitors (namely, SL-11144, SL-11156, and SL-11061) described by Maiale and co-workers.[6]

A previous analysis of the ZmPAO inhibition properties of agmatine derivatives suggested a hydrophobic substituent as the main determinant for inhibitory activity.[25,28] In fact, the addition of a lipophilic moiety (in particular, a prenyl substituent) to one of the terminal nitrogen atoms of the guanidine group of **2** (Table 1) greatly increased the inhibitory activity of about 200-fold (compare **2** and its *N*-prenyl analogue **3**), owing to the presence of a hydrophobic pocket located at the wide catalytic tunnel opening of ZmPAO, able to bind the prenyl group with high affinity.[25] Consistently, the significant reduction of the hydrophobic pocket could explicate the lower affinity displayed by **3**, **17**, and MDL 72527 for N^1-acetyl-PAO (APAO) and SMO compared to ZmPAO.[24] Moreover, the lengthening of the aliphatic chain from four (**3**) to five and six (**4** and **5**, respectively) carbon atoms did not significantly affect activity, although **4** was found to be the most potent agmatino-like derivative, according to the evidence that the ZmPAO catalytic tunnel is a favorable hydrophobic environment for the binding of aliphatic molecules of variable length.[22]

On the basis of these results, **4** was kept as a molecular template to further investigate the structure−activity relationships of agmatine analogues by design and synthesis of second generation derivatives. In particular, some of them, with the aminopentyl chain unchanged, were obtained by replacement of the prenyl group with various saturated and unsaturated rings (**10**−**13**) and designed to explore the ability of the hydrophobic pocket of ZmPAO to accommodate lipophilic groups different from the prenyl substituent of **4**. The remaining inhibitors **14**−**16** were characterized by modifications of the aliphatic chain, while the prenyl group on guanidine was kept fixed.

Moreover, during the fulfilment of this project, a LC−MS methodology was developed for the analysis of guazatine,[29] a nonsystemic contact fungicide that disturbs the membrane function of fungi and that is commercially available as a complex mixture of polyamines and guanidines. Several of the mixture components, already studied for their antifungal properties,[29] were tested for their ability to inhibit ZmPAO.

Table 1. Structures of Agmatine and Iminoctadine Derivatives and Their Affinity toward ZmPAO

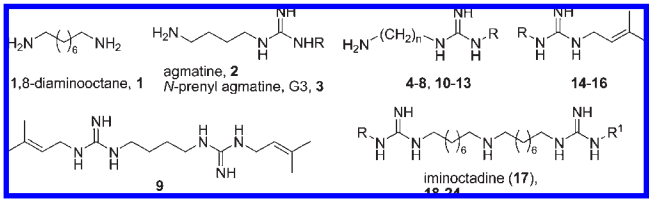

Compd	n	R	R^1	K_i (nM)[a]
1,8-diaminooctane, **1**				300
agmatine, **2**		H		3000
N-prenyl agmatine, G3, **3**				15
4	5			10
5	6			22
6	4			130
7	4	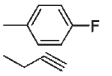		630
8	4			250
9				1500
10	5	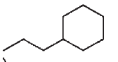		1720
11	5			2580
12	5	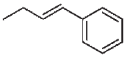		1530
13	5	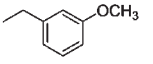		1150
14		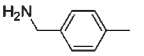		18000
15		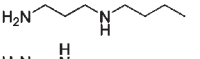		1210
16		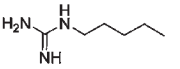		700
Iminoctadine, **17**		H	H	7.5
18		H		3.0
19		H		0.08
20		H	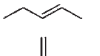	1.1
21		H		0.5
22		H	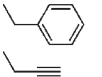	1.0
23		H	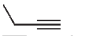	0.7
24			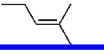	1.7

[a] In the experimental conditions utilized, since the lowest exploitable concentration of ZmPAO, as imposed by the enzyme assay sensitivity, is 0.2 nM, K_i values for ZmPAO inhibition by some of the iminoctadine derivatives (especially **19**) are overestimated and thus represent higher limit values.

Scheme 1[a]

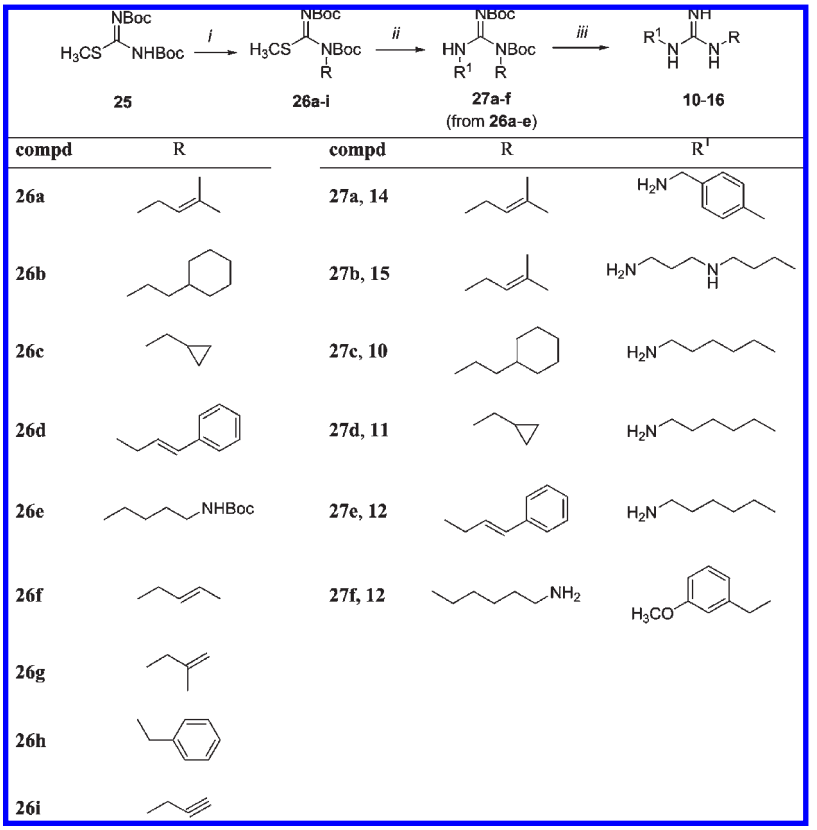

[a] Reagents and conditions. (i) For **26a** and **26g**: RBr, TBAB, KOK, CH_2Cl_2/CH_3CN, 19/1, room temp. For **26b**−**f** and **26h**,**i**: ROH, Ph_3P, DIAD, THF, 0 °C → reflux. (ii) For **27b**−**e**: R-NH_2, THF/H_2O, 50 °C. For **27a** and **27f**: R-NH_2, CH_3CN. (iii) CF_3COOH, CH_2Cl_2.

As a result, **17** (Table 1) showed K_i = 7.5 nM and was then used as the template to design a number of lipophilic derivatives (compounds **18**−**24**, Table 1) characterized by the presence of a hydrophobic terminal portion previously suggested to be important for the activity of ZmPAO inhibitors.

Chemistry

The *N*-Boc-protected *S*-methylisothiourea **2** (Scheme 1) was alkylated with the appropriate bromide by transfer phase catalysis to give the corresponding alkylated and protected *S*-methylisothioureas **26a** and **26g**, while compounds **26b**−**f** and **26h**,**i** were obtained by treating **25** with the appropriate alcohol under the Mitsunobu conditions. Compounds **26a**−**e** were then submitted to a nucleophilic displacement of the methylthio group by four different amines. While 1,5-pentanediamine and 4-aminobenzylamine were monoprotected before their use, the protection of bis(3-aminopropyl)amine was particularly troublesome, and for this reason it was used unprotected. Compounds **27b**−**e** were obtained in a good 80% yield starting from **26a**−**d** and using a slight excess of the amine in THF/H_2O at 50 °C. Guanylation of 4-aminobenzylamine and 3-methoxybenzylamine was accomplished in CH_3CN at room temperature, giving **27a** and **27f** with a 90% and 40% yield, respectively. Compound **28** (Scheme 2) was obtained in two steps starting from **26a**, which was initially reacted in a THF/H_2O mixture with a large excess of 1,4-diaminobutane to give the high polar intermediate **27g**, which was guanylated by reaction with **25**. Finally, the target compounds **10**−**16** were obtained by simple deprotection of the amino groups of **27a**−**g** using TFA in dry CH_2Cl_2. In some cases, becuase of the high number of protected amino groups in the molecule, multiple additions of TFA and long reaction times were necessary to drive the reaction to completion.

Scheme 2[a]

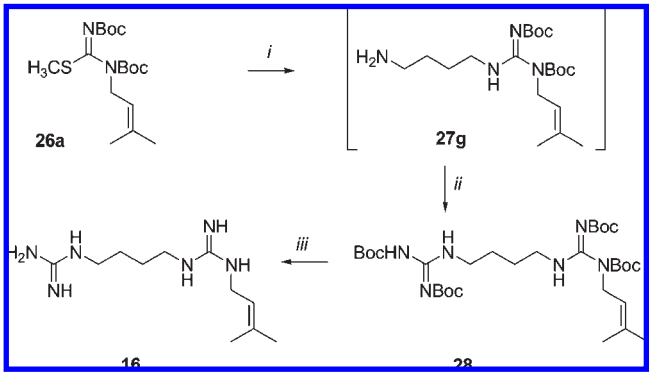

[a] Reagents and conditions: (i) 1,4-diaminobutane, THF/H_2O, 50 °C; (ii) **25**, THF/H_2O, 50 °C; (iii) CF_3COOH, CH_2Cl_2.

Compounds **18**−**24** (Scheme 3) were obtained starting from 2.6 equiv of 1,17-diamino-9-azaheptadecane (**29**), which was monoguanylated by the use of 1 equiv of the appropriate **26** to give the intermediates **30a**−**f**. These compounds were then submitted to a second guanylation step in the presence of 1,3-bis(*tert*-butoxycarbonyl)-2-triflylguanidine, affording the Boc-protected derivatives **31a**−**f**. On the other hand, treatment of 1 equiv of **29** with 2 equiv of **26a** afforded **31g** in a single synthetic step. Deprotection of **31a**−**g** in the presence of 10% TFA in CH_2Cl_2 gave the final compounds **18**−**24**.

Scheme 3[a]

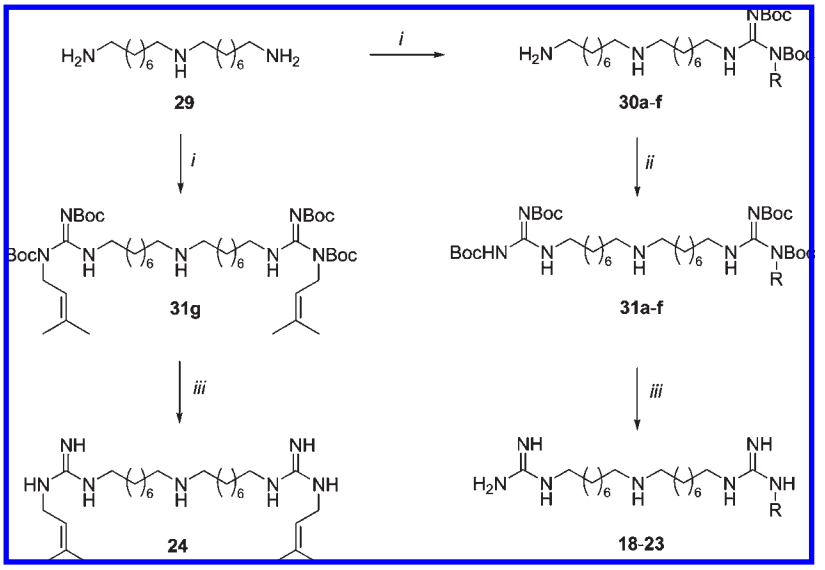

[a] Reagents and conditions. (i) For **30a**−**f**: 0.4 equiv of **26a** or **26c** or **26f**−**i**, THF/MeOH, 50 °C, 16 h. For **31g**: 2 equiv of **26a**, THF/MeOH, 50 °C, 16 h. (ii) 1,3-Bis(*tert*-butoxycarbonyl)-2-triflylguanidine, Et_3N, CH_2Cl_2, room temp, 6 h. (iii)10% TFA, CH_2Cl_2, room temp, 24 h.

Biological Assays

ZmPAO was purified as previously described.[4] Enzyme activity was measured spectrophotometrically by following the formation of a pink adduct resulting from the H_2O_2-dependent oxidation of 4-aminoantipyrine catalyzed by horseradish peroxidase and the subsequent condensation of oxidized 4-aminoantipyrine with 3,5-dichloro-2-hydroxybenzenesulfonic acid.[30] ZmPAO activity was assayed at pH 6.5 with Spd as the substrate in the presence or absence of test compounds. K_i values were determined according to the Dixon graphical method[31] (see also Supporting Information).

Results and Discussion

Inhibition of ZmPAO by Agmatine and Iminoctadine Derivatives. Agmatine (**2**) and its analogues (**3**−**9**) competitively inhibited Spd oxidation catalyzed by ZmPAO.[27,28] The presence of a prenyl substituent on the guanidine moiety (**3**−**5**) was the major determinant of the inhibitory activity because of the presence of a hydrophobic pocket in the ZmPAO active site, which is able to bind the prenyl group with high affinity.[25]

Considering that **4** (K_i = 10 nM)[28] had proved to be the most active compound among the analogues of **3**, we designed and synthesized compounds **10**−**13** with the five-membered alkylamino chain kept fixed while the prenyl moiety was replaced with cycloaliphatic or unsaturated/aromatic groups. They showed comparable inhibitory activity (K_i values spanning from 1150 to 2580 nM) but were more than 2 orders of magnitude less active than the parent compound **4**, thus indicating the prenyl group as the optimal substituent and suggesting a high selectivity of the hydrophobic binding pocket in accommodating lipophilic substituents of different nature. On the other hand, with the prenyl substituent fixed on the guanidine and with modification of the aminoalkyl portion of the molecule, the best result was obtained with a 4-membered alkyl chain bearing a terminal guanidine moiety (**16**, K_i = 700 nM) and with the introduction of a secondary nitrogen atom in a seven-membered alkyl chain (**15**, K_i = 1210 nM), while a benzylamino group (**14**) produced a significant reduction of affinity (K_i = 18 000 nM).

Excellent results were obtained with the series of iminoctadine (**17**) analogues. Iminoctadine, a component of the guazatine mixture, strongly inhibited ZmPAO activity with a K_i value of 7.5 nM, identical to that previously reported for the guazatine mixture.[27] In particular, the introduction of a prenyl chain on one of the guanidine moieties of **17** led to **18** showing a very high affinity toward the enzyme, with a K_i value in the nanomolar range (3.0 nM). The introduction of a second prenyl group as in **24** (K_i = 1.7 nM), as well as changing the prenyl chain of **17** with different unsaturated moieties such as a γ-methylallyl (**20**, K_i = 1.1 nM), a propargyl (**23**, K_i = 0.7 nM), and a β-methylallyl group (**21**, K_i = 0.5 nM), slightly ameliorated the affinity of the molecules with respect to the parent compound. Moreover, replacement of the prenyl chain of **17** with a cyclopropylmethyl substituent resulted in **19** with K_i = 0.08 nM. On the basis of its affinity, compound **19** is the most potent inhibitor of ZmPAO reported so far. Finally, a benzyl chain instead of the prenyl group of iminoctadine led to **22**, which retained nanomolar affinity (K_i = 1.0 nM).

In summary, compounds **3**−**5** (Table 1) appeared to be the most potent inhibitors among agmatine analogues (**2**−**16**) while compounds belonging to the class of iminoctadine-like inhibitors (**18**−**24**) showed similar potency, comparable to or higher than that of iminoctadine itself.

Prediction of Pharmacokinetic Properties. Several physicochemical properties (octanol/water partition coefficient, aqueous solubility, apparent Caco-2 cell permebility, and percent of human oral absorption) of the new PAO inhibitors were predicted (QikProp software)[32] to assess for their druglikeness (Table 2). All the inhibitors showed a log *P* in the range of the recommended values (−2.0 and 6.5 define the range of log *P* values reported for 95% of known drugs). The predicted aqueous solubility (log *S*) was also optimal for all the molecules with the exceptions of **2** (out of the range) and **9** and **24** (borderline values). The predicted apparent Caco-2 cell permeability value (P_{Caco}, an additional parameter of permeability that is used as a model for the gut−blood barrier)[33] was < 25 nm/s for **2**, **15**, **17**, **18**, **20**−**23** (suggesting poor permeability) and 25−500 nm/s for the

Table 2. Predicted Physicochemical Parameters of Compounds **1**−**24**

compd	log $P_{o/w}$ [a]	log S [b]	P_{Caco} [c]	human oral absorption (%)[d]
1	1.04	−0.42	688.03	70.84
2	−1.42	0.85	23.51	30.20
3	0.99	−1.22	128.48	70.10
4	1.36	−1.89	125.05	72.47
5	1.65	−2.03	121.43	73.92
6	0.36	−0.36	134.30	67.13
7	1.61	−1.72	146.03	75.10
8	0.08	−0.11	125.66	64.97
9	3.51	−6.22	378.84	80.66
10	2.11	−2.34	168.20	79.13
11	0.94	−0.61	227.12	74.63
12	2.31	−2.62	150.10	79.44
13	1.90	−1.70	295.90	82.31
14	1.46	−2.15	118.32	72.59
15	0.58	−0.62	23.39	41.90
16	0.81	−2.26	145.09	57.40
17	1.47	−3.21	13.29	30.65
18	3.97	−6.0	2.82	57.35
19	3.33	−3.92	25.60	58.68
20	3.57	−4.94	17.37	57.10
21	3.61	−4.90	20.48	58.61
22	4.23	−5.58	19.41	61.80
23	3.05	−4.76	13.14	51.85
24	6.18	−6.51	146.86	76.03

[a] Predicted octanol/water partition coefficient (−2.0 and 6.5 define the range of log P values reported for 95% of known drugs). [b] Predicted aqueous solubility in mol·dm^{-3} is the concentration of the solute in a saturated solution that is in equilibrium with the crystalline solid (−6.5 and 0.5 define the range of log P values reported for 95% of known drugs). [c] Predicted apparent Caco-2 cell permeability in nm/s (<25, poor permeability; >500, great permeability). [d] Percentage of predicted human oral absorption (>80%, high absorption; <25%, poor absorption).

remaining compounds (suggesting moderate permeability). Only **1** was predicted to have a great permeability (P_{Caco} > 500 nm/s). The most active inhibitor (**19**) showed an optimal value for either log P or log S, and its Caco-2 cell permeability was predicted to be better than that of the other iminoctadine derivatives (with the exception of **24**), although quite poor.

Cell Growth and Viability Assay on 19. Compound **19**, the most active ZmPAO inhibitor reported in the literature, was also evaluated for its effect on cell growth and viability in tumor cells. The effectiveness in toxicity and in reducing cancer cell growth was demonstrated by MTT survival and Trypan blue assays on HeLa and U373-MG cell lines characterized by a high and low proliferation rate, respectively. In fact, cell proliferation, viability, and activity of mitochondrial electron transport chain were determined through the capacity of cells to reduce 3-(4,5-dimethylthiazol-2-yl)-2,5-diphenyltetrazolium bromide (MTT) to formazan, while the Trypan blue method was applied to distinguish between living and dead cells. Cell viability measured by MTT assay was significantly diminished in both cell lines upon treatment with 1 μM **19** for 48, 72, and 96 h (Figure 1, panels c and d). In addition, the Trypan blue dye exclusion assay suggested a cytostatic effect rather than toxic (Figure 1, panels a and b). However, a noticeable toxic effect was instead revealed at 10 μM (Figure 1, panels c and d), the lowest tested concentration that significantly induced cell death (in a similar way, it was previously demonstrated that other polyamine analogues could be cytotoxic at a 10 μM concentration).[34] Accordingly, Trypan blue count revealed a number of viable cells appreciably lower than relative control to zero time cell-plating (data not shown). Therefore,

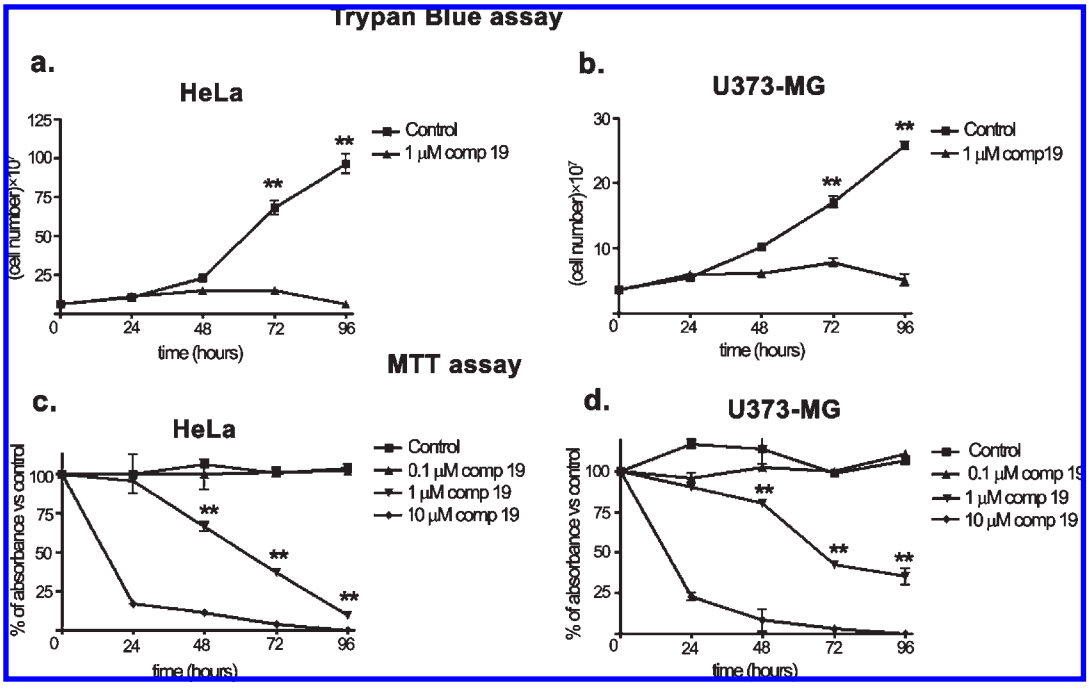

Figure 1. Measurement of living cell number: HeLa (a) and U373-MG (b) cells were incubated in the absence (control) or presence of 1 μM **19** for 0, 24, 48, 72, and 96 h. The addition of Trypan blue allows us to distinguish viable, unstained cells from nonviable, blue-stained cells. Data were expressed as (number of living cells) × 10^7. Statistical analysis was performed with a two-way ANOVA test comparing compound treatment versus control (**, $P < 0.001$ was considered as statistically significant). MTT evaluation of cells proliferation: HeLa (c) and U373-MG (d) cells were incubated in the absence (control) or presence of 0.1, 1, or 10 μM **19** and processed for MTT assay after 0, 24, 48, 72, and 96 h. The relative rate of cell proliferation was expressed as percent of absorbance versus untreated control. Statistical analysis was performed with a two-way ANOVA test. From a comparison of 1 μM compound treatment versus control, the MTT reduction rate gradually decreases, being statistically significant ($P < 0.001$) at 48−96 h.

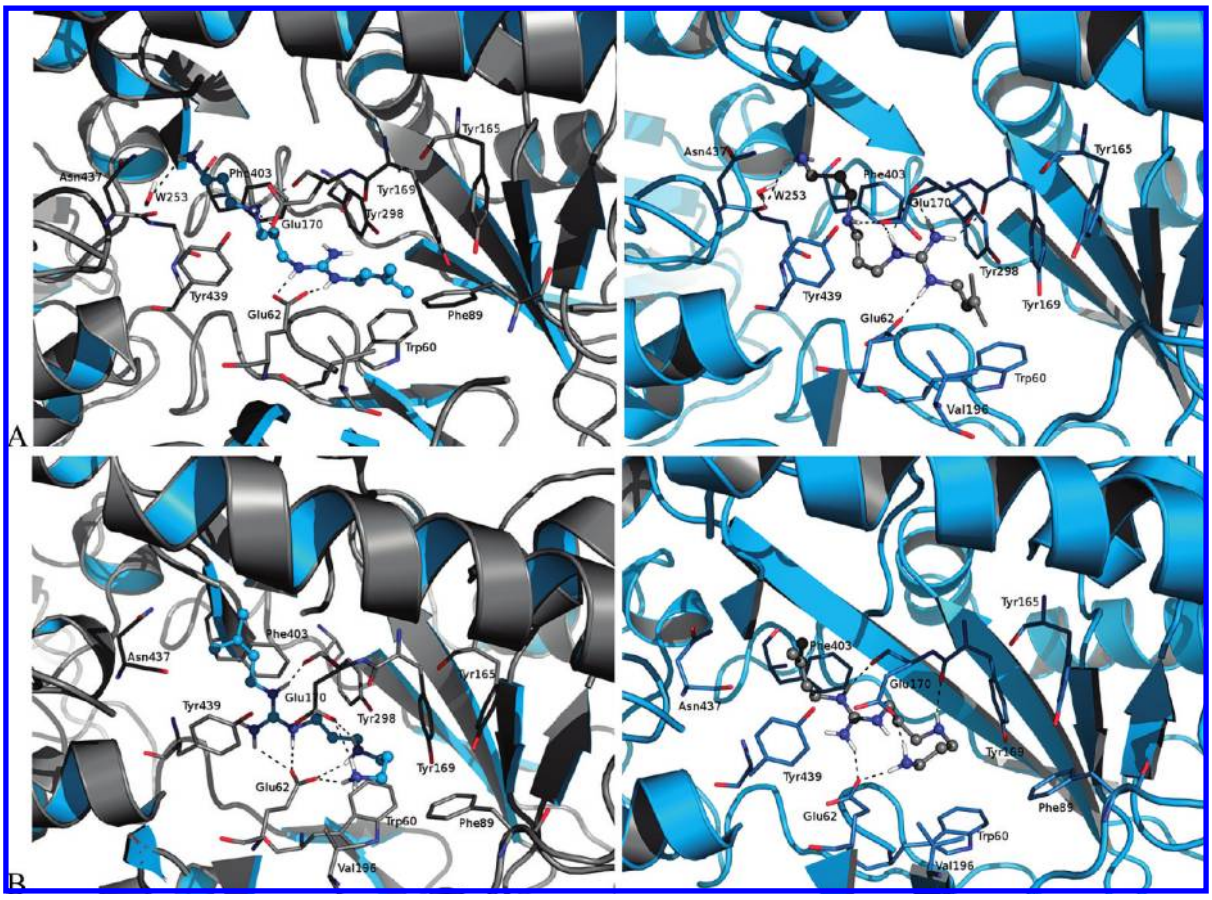

Figure 2. (A) Graphical representation of the binding mode of **15** in P orientation in both charged (left) and uncharged (right) forms. (B) L orientation of **15** in both charged (left) and uncharged (right) forms.

such a preliminary investigation demonstrated both toxic effects and inhibition of proliferation on U373-MG and HeLa cell lines treated with **19**. In particular, a 10 μM concentration was clearly toxic for tumor cells, already after a 24 h treatment (Figure 1, panels c and d), whereas a 1 μM concentration seemed to activate a significant blockage of cell proliferation.

Analysis of Binding Mode. As previously reported,[25] atomic coordinates of ZmPAO used in modeling simulations were derived from the structure of the complex between the enzyme and **17**, refined at 1.9 Å resolution,[22] that is, along with the 3D structure of yeast spermine amine oxidase,[35] the only member of the family whose tridimensional structure is known. One of the most striking features of ZmPAO is a 30 Å long, U-shaped catalytic tunnel that hosts the FAD isoalloxazine ring and the crucial catalytic residue Lys300, which is highly conserved in all the proteins of APAO and SMO families.[24] The tunnel shows two openings of different sizes. One of them, lined mainly by carboxylates of glutamic and aspartic residues (namely, Asp88, Asp90, Asp117, Glu120, Glu121, Glu124, Asp194, and Asp195) and forming the so-called "carboxylate ring", constitutes the large entrance of the tunnel. Differently, the second opening is too narrow to admit the ligands. As a consequence, both substrates and inhibitors can get into the tunnel only by passing the largest entrance. Moreover, since the tunnel has a diameter ranging between 3.8 and 4.3 Å,[21] the ligands cannot invert their orientation upon binding and are forced to keep the same orientation once they had entered the tunnel. The tunnel is mainly bordered by hydrophobic and aromatic residues, with the exception of Glu62 and Glu170, that protrude in front of the flavin and are within hydrogen bond distance from each other and from active site ligands. The Glu62−Glu170 pair may represent the structural element that properly aligns the substrate within the tunnel.[22] Aromatic residues such as Phe403, Tyr439, and Tyr298 are also crucial elements of the catalytic tunnel. The side chains of Phe403 and Tyr439 are positioned parallel to each other and flank the tunnel on opposite sites, forming an aromatic sandwich that makes interactions with enzyme-bound inhibitors. The Tyr298 side chain also appears within hydrogen bond distance from active site ligands.

Because of the uncertainty on the protonation state of ligands within the enzyme binding site, computer simulations on both the charged and uncharged forms of inhibitors have been performed. As an example, the protonated form of **15** showed its terminal charged edge directed toward the narrow entrance of the catalytic tunnel, suggesting that the ligand penetrated the tunnel through its terminal ammonium group (this binding mode is thereafter referred to as the P orientation, Figure 2A, left side. Further details on the binding mode of ZmPAO inhibitors are in Supporting Information).

In addition, among the conformers found by docking calculations, an opposite orientation (thereafter referred to as the L orientation, Figure 2 B, left side) into the catalytic tunnel, characterized by a comparable energy with respect to the global minimum, was also found. In detail, the prenyl group of **15** was located in proximity to the narrow entrance of the tunnel, while the guanidino moiety formed a cation−π interaction with the aromatic rings of Phe403 and Tyr439.

In contrast, simulations performed on the uncharged form of ligands led to results difficult to be interpreted. In fact, the P and the L orientations are both represented in the lower energy clusters, avoiding the identification of a significantly preferred orientation. The binding mode of unprotonated **15** in the L orientation (Figure 2 B, right side) is very similar to that found for its charged form, while the P orientation (Figure 2 A, right side) showed an interaction pattern within the catalytic tunnel that is slightly different (see Supporting Information).

Modeled complexes between docked inhibitors and the ZmPAO catalytic binding site allowed us to rule out a preliminary structure−affinity relationship of the new compounds. In particular, the major determinant for activity of agmatine derivatives **3**−**8** seemed to be their prenyl moiety that in general was accommodated within the hydrophobic pocket close to the large entrance of the tunnel, where the most profitable region of interaction with a C1= probe of GRID[36] was found (Figure 3). In fact, insertion of the prenyl group into the structure of agmatine (**2**) led to **3** with a 20-fold improved affinity, while replacement of the same moiety by different unsaturated cycloalkyl or aromatic groups (**6**−**8** and **10**−**13**) was detrimental for affinity, with K_i values at least 1 order of magnitude higher. This trend was accounted by docking calculations showing that hydrophobic substituents of **6**−**8** and **10**−**13** had shape and size that lack several contacts with the major hydrophobic pocket of the enzyme binding site. In contrast, variation of the length of the alkyl spacer from four to five and six carbon atoms (**4** and **5**, respectively) did not influence affinity, further supporting the hypothesis that the hydrophobic moiety of agmatine derivatives played a very important role in defining affinity of compounds. In agreement with that, compounds **4** and **5**, although characterized by longer alkyl chains with respect to **3**, showed similar interactions between their terminal ammonium group and glutamates 62 and 170 (hydrogen bonds) or aromatic residues (cation−π interactions) of the binding site.

On the other hand, keeping fixed the prenylguanidine moiety of **3** and replacing its aminobutyl terminal with various basic side chains, affinity underwent a 50- to 1200-fold decrease (**14**−**16**). The low affinity of **14** and **16** seemed to depend on the lack of a quaternary nitrogen atom (able to bind glutamates and to interact with aromatic residues as in **3**) acting as an anchor point to orientate the ligand within the binding pocket. In fact, docked complexes did not show a preferential binding mode for such compounds. On this basis, however, it is impossible to rationalize the affinity of **15** (1210 nM), which possessed such a structural feature and showed interactions similar to that of better compounds.

The importance of a protonatable nitrogen atom able to contact Glu62, Glu170, and near neighboring aromatic residues was also supported by the X-ray crystallographic structure of ZmPAO in complex with **17**, which showed such interactions. Moreover, the nanomolar affinity of **17** also depended on the long alkyl chains contacting aromatic residues of the catalytic tunnel and on cation−π interactions between guanidino groups and aromatic amino acids (all reproduced by docking simulations, thus giving support for the reliability of the computational protocol). Derivatives of **17**, obtained by insertion of a lipophilic moiety at one or both of its guanidino edges, were all characterized by affinity values better than that of the parent compound. As expected, the preferred orientation of docked complexes of iminoctadine

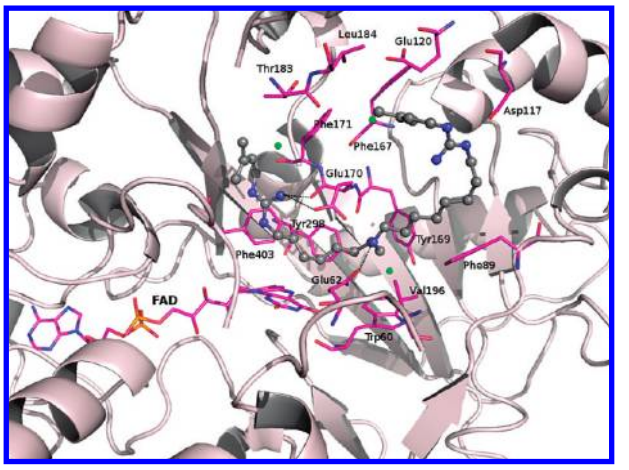

Figure 3. Graphical representation of the lowest energy ZmPAO−**24** complex (ball-and-stick notation, carbon atoms in cyan) as obtained by docking simulations. Regions of minimum energy as derived from molecular interaction field calculations are also displayed for the C1= probe (green spheres).

derivatives **18**−**24** suggested that they could penetrate the tunnel by their charged edge (the guanidine moiety), similar to agmatine derivatives, while the terminal lipophilic group was located within the hydrophobic pocket close to the large entrance of the tunnel. However, affinity values did not significantly depend on the lipophilic substituent, affinity ranging from 0.5 to 3 nM, with the sole exception of **19** (0.08 nM). This was probably due to the huge number of profitable interactions that iminoctadine derivatives made with the catalytic tunnel, much higher than those involving smaller molecules, such as prenylagmatine derivatives.

Compound **19**, which exhibited the highest activity among the new guanidine derivatives and, to the best of our knowledge, among all known ZmPAO inhibitors, penetrates the tunnel by means of the free guanidine moiety and, in addition to the polar interactions (see Supporting Information), it showed peculiar lipophilic contacts. In fact, after minimization, the χ angle of the side chain of Leu186 shifted from −82.73° to −145.17°, assuming a different rotameric state that created a hydrophobic pocket (defined by Ile140, Val184, Leu186, Phe167, and Phe171) not present in the crystallographic complex between ZmPAO and iminoctadine. This pocket, mapped by a GRID minimum of the DRY probe, allowed the cyclopropyl moiety to have very favorable lipophilic interactions (Figure 4). In particular, although the DRY probe identified the first part of catalytic tunnel as favorable for lipophilic contacts, three major interaction zones could be described: (1) a pocket lined by Trp60, Phe89, and Val196 interacting with one of the polymethylene spacer, (2) the region in front of the aromatic ring of Phe189, in contact with the second polymethylene spacer, and (3) the space between side chains of Leu186 and Phe171, accommodating the cyclopropyl moiety.

To check for the stability of the **19**−ZmPAO complex and of the lipophilic interactions between the cyclopropyl moiety and the pocket defined by Ile140, Val184, Leu186, Phe167, and Phe171, a molecular dynamics (MD) simulation was performed. During the initial steps of calculations, the hydrophobic interactions observed in the minimized complex were maintained, with the χ angle of Leu186 always found in a trans conformation. Next, such a dihedral angle shifted from a trans to a gauche+ conformation, thus

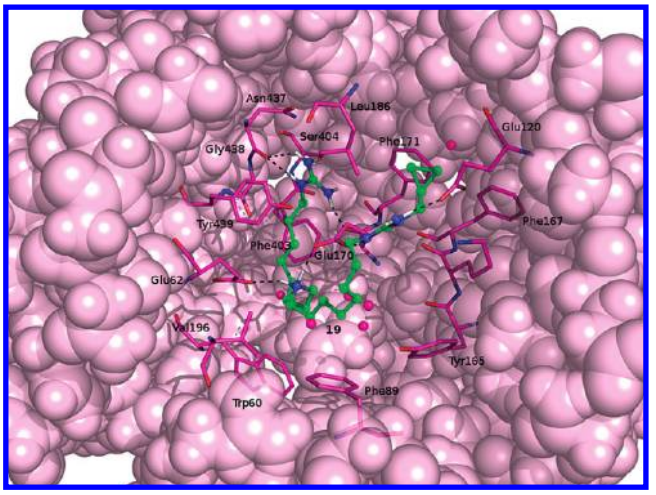

Figure 4. Binding mode of **19** (ball-and-stick notation, carbon atoms in green) into the ZmPAO catalytic binding site. Pink spheres represent regions of minimum energy as derived from molecular interaction field calculations with the GRID DRY probe. Intermolecular hydrogen bonds are represented as black dashed lines. Residues lining the catalytic tunnel are shown.

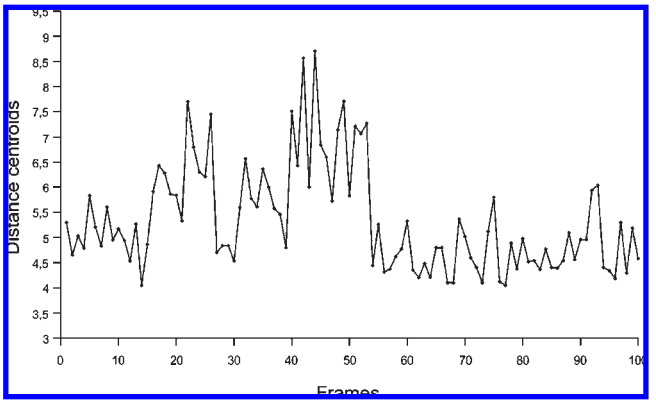

Figure 5. Distance between the centroids of aromatic ring of Phe171 and cyclopropyl moiety of compound **19** during the course of molecular dynamics simulations.

opening a gap that allowed the cyclopropylmethyl moiety to penetrate more deeply into the lipophilic pocket and to make a profitable stacked interaction with the aromatic ring of Phe171, as shown in Figure 5, depicting the distance in Å between the centroid of the Phe171 ring and the cyclopropyl group versus the frames of the MD run. Such a result confirmed the importance of the lipophilic interactions with Leu186 and Phe171 (found by docking simulations and by GRID calculations). In fact, despite the high flexibility of **19** and the wide size of the catalytic tunnel entrance, the cyclopropyl moiety maintained lipophilic interactions and, upon large fluctuations found from the beginning to the middle of the simulation (Figure 5), it was also able to reinforce contacts with Phe171.

Compound **24**, bearing a prenyl group at each of its molecular edges, interacted by the guanidino moieties with Asp117 and Glu170, while the secondary amino group formed a hydrogen bond with the side chain of Glu62. Prenyl moieties contacted two of the three zones preferred by the C1= probe (Figure 3), corresponding to Phe171, Leu184, and Thr183 (−4.0 kcal/mol) and to Phe171, Glu120, and Phe167 (−3.7 kcal/mol), although the most profitable interactions (−4.3 kcal/mol) for such a probe was found in a region close to Phe89, Trp60, and Tyr169, inaccessible to prenyl groups.

In summary, docking simulations and GRID calculations further support the hypothesis that the protonated form of inhibitors could be preferential with respect to the corresponding uncharged form, in agreement with that previously found by us on agmatine derivatives,[24] as well as suggested that charged inhibitors preferentially approached the tunnel through their charged terminal moiety (P orientation).

Moreover, while the prenyl moiety and the terminal amino group of agmatine derivatives appeared as the crucial keys for affinity, lipophilic terminal moieties of iminoctadine analogues should be considered as structural elements for fine-tuning of affinity toward the enzyme.

In conclusion, previous studies on agmatine derivatives suggested structural modifications to improve affinity of compounds toward PAO. New agmatine and iminoctadine analogues have been synthesized and tested for their inhibitory properties against maize polyamine oxidase, allowing us to identify a hit compound found to be the most potent inhibitor known so far (K_i = 0.08 nM). Because of the great interest devoted to PAOs and their inhibitors in cell proliferation and death in normal and cancer cells, the new compounds described in this paper could be considered as very interesting hits in the search of new agents able to inhibit cell proliferation in particular tumor cell lines. However, although the global fold of computational models previously reported for several plant and animal PAOs strictly resembles that of ZmPAO,[23] we are aware of the fact that structural differences might occur at their binding pockets, thus leading compounds to have different affinity toward these enzymes. On the basis of these considerations and on the lack of PAO structures from experimental sources (except for ZmPAO and yeast Fms1), additional efforts should be made to generate reliable models of mammalian and human PAO to be used for the design of new enzyme inhibitors and for rationalizing pre-existing biological data.

Experimental Section

Chemistry. Starting materials were purchased from Aldrich-Italia (Milan, Italy). Melting points were determined with a Buchi 530 apparatus and are uncorrected. ^{1}H NMR spectra were recorded on a Varian Gemini 200 (200 MHz) instrument. Chemical shifts are reported as δ (ppm) relative to TMS as internal standard, and J is in Hz. ^{1}H patterns are described using the following abbreviations: s = singlet, d = doublet, t = triplet, m = multiplet, b = broad. Analyses for C, H, N were within ±0.4% of the theoretical value. No residue remained after combustion, thus indicating a purity of > 95%.

General Procedure for the Synthesis 26a and 26g. To a suspension of KOH (157 mg, 2.8 mmol) in a CH_2Cl_2/CH_3CN (19/1) mixture (3.5 mL) were added tetrabutylammonium bromide (65 mg, 0.2 mmol) and *N,N′*-bis(*tert*-butoxycarbonyl)-*S*-methylisothiourea (290 mg, 1 mmol). After a few minutes, a solution of the appropriate bromide (2.4 mmol) in CH_2Cl_2/CH_3CN (19/1, 3.5 mL) was added dropwise and the reaction mixture was stirred at room temperature for 16−18 h. The reaction mixture was poured into ice, and the aqueous layer was extracted once with CH_2Cl_2. The organic phase was washed with brine and dried over Na_2SO_4. The solvent was evaporated under reduced pressure, and the crude mixture was purified by flash chromatography.

***N*^{1},*N*^{2}-Bis(*tert*-butoxycarbonyl)-*N*^{1}-(*γ*,*γ*-dimethylallyl)-*S*-methylisothiourea (26a).** Reaction time: 16 h. Oil, 70% yield. ^{1}H NMR ($CDCl_3$, 200 MHz) δ 5.14−5.10 (m, 1H), 4.0−3.97 (m, 2H), 2.22 (s,

3H), 1.58−1.54 (m, 6H), 1.36 (s, 9H), 1.33 (s, 9H). MS (ESI) *m/z*: 739.1 $(2M + Na)^+$, 381.0 $(M + Na)^+$, 359.1 $(M + H)^+$.

N^1,N^2-Bis(*tert*-butoxycarbonyl)-N^1-(β-methylallyl)-*S*-methylisothiourea (26g). Reaction time: 18 h. Oil, 75% yield. ^{1}H NMR ($CDCl_3$, 200 MHz) δ 4.63 (s, 2H), 4.05 (s, 2H), 2.30 (s, 2H), 1.68 (s, 3H), 1.44 (s, 9H), 1.40 (s, 9H). MS (ESI) *m/z*: 710.9 $(2M + Na)^+$, 367.0 $(M + Na)^+$, 345.1 $(M + H)^+$.

General Procedure for the Synthesis 26b−f and 26h,i. To a stirred solution of *N*,*N*′-bis(*tert*-butoxycarbonyl)-*S*-methylisothiourea (2.90 g, 10 mmol) in dry THF (36 mL) were added Ph_3P (3.93 g, 15 mmol) and the appropriate alcohol (13 mmol). The reaction mixture was cooled to 0 °C, and DIAD (2.95 mL, 15 mmol) was added dropwise. After being stirred at reflux temperature for 17 h, the reaction mixture was concentrated and diluted with H_2O and CH_2Cl_2, the aqueous layer was extracted twice with CH_2Cl_2, and the combined organic phases were washed with brine and dried over Na_2SO_4. The solvent was evaporated under reduced pressure, and the crude mixture was purified by flash chromatography.

Example. N^1,N^2-Bis(*tert*-butoxycarbonyl)-N^1-(cyclohexylethyl)-*S*-methylisothiourea (26b). Yellow oil, 95% yield. ^{1}H NMR ($CDCl_3$, 200 MHz) δ 3.53−3.45 (m, 2H), 2.34 (s, 3H), 1.79−1.40 (m, 6H), 1.47 (s, 9H), 1.44 (s, 9H), 1.32−1.08 (m, 5H), 1.05−0.86 (m, 2 H).

General Procedure for the Synthesis 27a and 27f. To a solution of **26** (4 mmol) in CH_3CN (10 mL) was added the appropriate amine (1 mmol), and the reaction mixture was stirred for 16 h at room temperature. After removal of the solvent, the residue was partitioned between CH_2Cl_2 and H_2O and the aqueous layer was extracted twice with CH_2Cl_2. The combined organic phases were washed with brine and dried over Na_2SO_4. Removal of the solvent under vacuum gave a residue which was purified by flash chromatography.

N^1-Benzylamine-N^3-(γ,γ-dimethyallyl)-N^2,N^3,N^4-tris(*tert*-butoxycarbonyl)guanidine (27a). Oil, 92% yield. ^{1}H NMR ($CDCl_3$, 200 MHz) δ 7.29−6.94 (m, 4H), 5.26 (m, 1H), 4.39−4.12 (m, 4H), 1.70 (s, 3H), 1.66 (s, 3H), 1.51 (s, 9H), 1.45 (s, 9H), 1.43 (s, 9H).

N^1-(3-Methoxybenzyl)-N^3-(5-aminopentyl)-N^2,N^3,N^4-tris(*tert*-butoxycarbonyl)guanidine (27f). Oil, 56% yield. ^{1}H NMR ($CDCl_3$, 200 MHz) δ 7.29−6.72 (m, 4H), 4.36 (s, 2H), 3.78 (s, 3H), 3.64−3.52 (m, 2H), 3.12−3.29 (m, 2H), 1.65−1.42 (m+3s, 33H).

Synthesis of N^1-[(3′-Aminopropyl)-3-aminopropyl]-N^3-(γ,γ-dimethylallyl)-N^2,N^3-bis(*tert*-butoxycarbonyl)guanidine (27b). To a solution of *N*-(3-aminopropyl)-1,3-propanediamine (1.2 mL, 8.37 mmol) in a 50/1 THF/H_2O mixture, a solution of **26a** (1.00 g, 2.79 mmol) in THF (15 mL) was added dropwise over 1 h. The reaction mixture was heated at 50 °C for 3 h, and then it was concentrated under vacuum and diluted with H_2O and CH_2Cl_2. The aqueous phase was extracted twice with CH_2Cl_2. Then the combined organic solutions were washed with brine and dried over Na_2SO_4. The residue obtained after the removal of the solvent was purified by flash chromatography to give **27b** (689 mg, 56% yield) as a yellow oil. ^{1}H NMR ($CDCl_3$, 200 MHz) δ 5.10 (t, *J* = 6.9 Hz, 1H), 4.11 (d, *J* = 7.0 Hz, 2H), 3.62−3.48 (m, 1H), 3.34−3.05 (m, 3H), 2.69−2.47 (m, 4H), 1.68−1.47 (m, 10 H), 1.38 (s, 9H), 1.36 (s, 9H).

General Procedure for the Synthesis of 27c−e. To a solution of *N*-(*tert*-butoxycarbonyl)-1,5-pentandiamine (1.17 g, 5.81 mmol) in THF (10 mL) was added dropwise a solution of **26** (2.90 mmol) in THF (10 mL), and the reaction mixture was heated at 50 °C for 18 h. After removal of the solvent, the residue was partitioned between CH_2Cl_2 and H_2O and the aqueous phase was extracted twice with CH_2Cl_2. The combined organic phases were washed with brine and dried over Na_2SO_4. The residue obtained after removal of the solvent was purified by flash chromatography to give the desired pure products.

Example. (N^1-5-Aminopentyl)-N^3-(cyclohexylethyl)-N^1,N^2,N^3-tris(*tert*-butoxycarbonyl)guanidine (27c). Oil, 95% yield. ^{1}H NMR ($CDCl_3$, 200 MHz) δ 3.69−3.54 (m, 2H), 3.21−3.11 (m, 4H), 1.73−1.12 (m+3s, 44H), 0.98−0.80 (m, 2H).

Synthesis of 4-[N^2,N^3-Bis(*tert*-butoxycarbonyl)-N^3-(γ,γ-dimethylallyl)guanidine]-1-[N^5,N^6-bis(*tert*-butoxycarbonyl)guanidino]-butane (28). To a solution of 1,4-diaminobutane (739 mg, 8.38 mmol) in a THF/H_2O, 50/1, mixture (20 mL) was added dropwise a solution of **26a** (1.00 g, 2.79 mmol) in THF (15 mL), and the reaction mixture was heated at 50 °C for 3 h. After removal of the solvent, the residue was partitioned between CH_2Cl_2 and 10% $NaHCO_3$ and the aqueous layer was extracted twice with CH_2Cl_2. The combined organic phases were washed with brine and dried over Na_2SO_4, and the residue obtained by removal of the solvent was dissolved in a THF/H_2O, 50/1, mixture. To this solution, a solution of **25** (0.81 g, 2.79 mmol) in THF (10 mL) was added dropwise, and the reaction mixture was heated at 50 °C for 16 h. The residue obtained by standard workup using CH_2Cl_2 and H_2O was purified by flash chromatography to give **6** (0.625 g, 35% yield) as a brown oil. ^{1}H NMR ($CDCl_3$, 200 MHz) δ 5.28−5.12 (m, 1H), 4.26−4.14 (m, 2H), 3.28−3.02 (m, 4H), 1.78−1.26 (m+4s, 46H).

General Procedure for the Synthesis of 10−16. Freshly distilled CF_3COOH (0.917 mL, 12.28 mmol) was added to a solution of **27** (for **10−15**) or **28** (for **16**) (1 mmol) in dry CH_2Cl_2, and the reaction mixture was stirred at room temperature for 3−16 h depending on the number of protecting groups to be removed. Removal of the solvent under vacuum gave a residue which was washed with several times petroleum ether to give **10−16** as pure compounds.

Example. N^1-Benzylamine-N^3-(γ,γ-dimethylallyl)guanidine Bis(trifluoroacetate) (14). Oil, 99% yield. ^{1}H NMR (CD_3OD, 200 MHz) δ 7.54 (d, *J* = 8.56 Hz, 2H), 7.36 (d, *J* = 8.59 Hz, 2H), 5.30−5.27 (m, 1H), 4.12 (s, 2H), 3.87 (d, *J* = 6.74 Hz, 2H), 1.71 (s, 3H), 1.62 (s, 3H). MS (EI) *m/z* 233 (M + H).

General Procedure for the Synthesis of 30a−f. To a stirred solution of 1,17-diamino-9-azaheptadecane (4.08 g, 15.06 mmol) in 5/3 THF/CH_3OH (80 mL) at 50 °C, a solution of *N*,*N*′-bis(*tert*-butoxycarbonyl)-*N*-(alkyl)-*S*-methylisothiourea (5.02 mmol) in THF (25 mL) was added dropwise over 1 h. After 18 h, the reaction mixture was concentrated under reduced pressure and the residue was purified by flash chromatography (6% methanol, 4% triethylamine, 90% ethyl acetate), affording pure **30a−f**.

Example. 1-Amino-17-(N^1,N^2-bis(*tert*-butoxycarbonyl)-N^1-(γ,γ-dimethylallyl)guanidine)-9-azaheptadecane (30a). Oil, 80% yield. ^{1}H NMR ($CDCl_3$, 200 MHz) δ 7.22 (bs, NH), 5.13 (t, *J* = 6,6 Hz, 1H), 4.15−4.12 (m, 2H), 3.05−2.98 (m, 2H), 2.61−2.46 (m, 6H), 1.60−1.58 (m, 6H), 1.45−1.42 (m, 22H), 1.32 (bs, 20H). MS (ESI) *m/z* 582 $(M + H)^+$.

General Procedure for the Synthesis of 31a−g. Et_3N (67 μL, 0.48 mmol) and 1,3-bis(*tert*-butoxycarbonyl)-2-triflylguanidine (188 mg, 0.48 mmol) were added to a stirred solution of **30** (0.44 mmol) in CH_2Cl_2 (8 mL), and the mixture was stirred at room temperature for 6 h. The mixture was concentrated under reduced pressure and purified by flash chromatography ($MeOH/Et_3N/EtOAc$, 3/2/95), affording **31a−g** as pure compounds.

Example. 1-(N^1,N^2-Bis(*tert*-butoxycarbonyl)guanidine)-17-(N^1,N^2-bis(*tert*-butoxycarbonyl)-N^1-(γ,γ-dimethylallyl)guanidine)-9-azaheptadecane (31a). Oil, 82% yield. ^{1}H NMR ($CDCl_3$, 200 MHz) δ 8.20 (bs, NH), 5.13 (t, *J* = 6.21 Hz, 1H), 4.21−4.18 (m, 2H), 3.25−3.18 (m, 4H), 3.12−3.05 (m, 2H), 2.79−2.66 (m, 4H), 1.65−1.63 (m, 6H), 1.46−1.43 (m, 44H), 1.27 (bs, 16H). MS (ESI) *m/z* 824 $(M+H)^+$.

General Procedure for the Synthesis of 18−24. A 10% solution of freshly distilled TFA in anhydrous CH_2Cl_2 (3 mL) was added to **31** (0.102 mmol) under argon atmosphere. The reaction mixture was stirred at room temperature for 24 h and concentrated under reduced pressure to give **18−24** in quantitative yield.

Example. 1-(Guanidino)-17-(N^1-(γ,γ-dimethylallyl)guanidino)-9-azaheptadecane tris(trifluoroacetate) (18). Oil. ^{1}H NMR

($(CD_3)_2CO$, 200 MHz) δ 8.62 (bs, NH), 7.85 (bs, NH), 7.32 (bs, NH), 5.25−5.23 (m, 1H), 3.41−3.32 (m, 2H), 3.73−3.65 (m, 2H), 3.41−3.35(m, 2H), 3.05−2.96 (m, 4H), 1.69−1.65 (m, 6H), 1.63 (bs, 8H), 1.45 (bs, 16H). MS (ESI) m/z 424 $(M + H)^+$.

Enzyme Activity and Inhibition Assays. ZmPAO was purified as previously described.[4] The ZmPAO activity was measured spectrophotometrically by following the formation of a pink adduct ($\varepsilon_{515nm} = 2.6 \times 10^4\ M^{-1}\ cm^{-1}$) as the result of the H_2O_2-dependent oxidation of 4-aminoantipyrine (Sigma-Aldrich) catalyzed by horseradish peroxidase (Sigma-Aldrich) and the subsequent condensation of oxidized 4-aminoantipyrine with 3,5-dichloro-2-hydroxybenzenesulfonic acid (Sigma-Aldrich).[30]

The ZmPAO activity was assayed at pH 6.5 (0.2 M sodium phosphate buffer) and 25 °C with Spd as the substrate in the presence or absence of test compounds. Enzyme activities were expressed in International Units (U; 1 unit is the amount of enzyme that catalyzes the oxidation of 1 μmol of substrate per minute). In the enzyme assays, the ZmPAO concentration ranged from 0.2 to 4.0 nM (i.e., [E] < [S] and [E] < [I], where [E], [S], and [I] represent the enzyme, substrate, and inhibitor concentrations, respectively), while the substrate concentration ranged from $0.1K_m$ to $10K_m$ (where K_m is the Michaelis constant). Specifically, Spd concentration ranged from 0.5 to 4 10^{-5} M, while ZmPAO concentration ranged from 0.2 to 0.7 nM for **17** and its derivatives **18**−**24** and from 1 to 4 nM for agmatine analogues **10**−**16**. Moreover, the inhibitor concentration ranged from $0.1K_i$ to $10K_i$ (where K_i is the apparent dissociation equilibrium constant for the formation of the reversible enzyme−inhibitor complex).

The initial reaction rate for the ZmPAO catalyzed conversion of the substrate was unaffected by the ZmPAO/inhibitor incubation time, prior to substrate addition. K_i values were determined according to the Dixon graphical method.[31] The data reported are the average of values obtained in three different experiments, each with two replicates. Standard error for each point was less than 8%.

Colorimetric MTT Assay and Trypan Blue Exclusion Test of Cell Viability. Human solid tumor U373-MG (glioblastoma/astrocytoma) and cervical carcinoma HeLa cell lines were seeded in Dulbecco's modified Eagle's medium (DMEM) and 10% FBS (Lonza) in 96-well plates (100 μL/well at a density of 2.5×10^3 cells/well). Cells were allowed to adhere and then exposed to various concentrations of the test compound **19** (0.1−10 μM) for 24, 48, 72, and 96 h. MTT assay (Sigma-Aldrich) was performed as indicated by the manufacturer's instructions at the end of each incubation period. The optical density (OD) of each sample was measured by an ELISA reader at 550 nm.[37] Cell viability was calculated according to [(OD of drug treatment)/(OD of control)] × 100. The dye exclusion test with Trypan blue, in association with MTT assay, was used to determine the number of U373-MG and HeLa living cells present after treatments with the compound. Trypan blue (Sigma-Aldrich) staining was performed according to routine procedures. Cells of each sample were counted two times in a Neubauer chamber, and the assay was performed in duplicate. The dye-excluding cells were indicated as the number of viable cells. All the experiments were performed independently at least three times.

Computational Details. All calculations and graphical manipulations were performed on Linux computers using the software packages Autodock 3.0.5[38] and MacroModel 8.5.[39] Atomic coordinates of ZmPAO used during molecular modeling simulations were derived from the structure of the complex between ZmMPAO and **17**[22] (1.9 Å resolution, RCSB Protein Data Bank entry 1H82). To set the initial coordinates for the docking studies, the residues belonging to chains A and B, two *N*-acetyl-D-glucosamine, two α-D-fucose, and two α-D-mannose residues present in the C chain of the crystal structure of ZmPAO were removed and excluded from all calculations. Similarly, the crystallographic water molecules were removed from the complex, with the exception of the following molecules which were considered in all the calculations (reported in parentheses is the numeration of the corresponding water molecules of complex ZmMPAO−1,8-diaminooctane used to validate the docking protocol; see below): (i) HOH158 (HOH148), present in the oxidized enzyme in the proximity of Lys300 and the N5 atom of FAD and constituting the so-called Lys300/water/flavin N5 motif; (ii) HOH253 (HOH247) and HOH94 (HOH84), found at the entrances of the catalytic site in the proximity of Asn437 and Tyr165, respectively, and (iii) HOH10 (HOH9), HOH23 (HOH263), HOH232 (HOH224), HOH264 (HOH261), HOH265 (HOH2), and HOH266 (HOH262), located in the FAD binding site. Hydrogen atoms were added to their idealized positions using Maestro[40] in such a way to protonate all the guanidino and amino groups of Arg and Lys residues, as well as both the N-terminal primary amino groups and the guanidino moieties of the inhibitors, and to deprotonate all the carboxy groups of Glu and Asp side chains, as well as the C-terminal carboxy group.[41]

The atomic partial charges for the inhibitors and for the cofactor FAD present in the catalytic tunnel of ZmMPAO were calculated with MOPAC using the AM1 approximation.

The program Autodock was used to evaluate the binding mode of the inhibitors and to explore their binding conformations within the ZmPAO structure. A grid point spacing of 0.375 Å and 90×90×90 points were used. The grid was centered on the macromolecule. Parameters for docking runs are reported in Supporting Information.

A different protocol was applied for the inhibitors with more than eight degrees of freedom. In particular, a series of separate calculations were performed and all the results of the single docking runs were merged and clustered with a 1.5 Å rms tolerance.

Next, on the basis of the fact that Autodock does not perform any structural optimization and energy minimization of the complexes found, a molecular mechanics/energy minimization (MM/EM) approach was applied to refine the Autodock output. The computational protocol applied consisted of the application of 100 000 steps of the Polak−Ribière conjugate gradients (PRCG) or until the derivative convergence was 0.05 kJ/mol. Moreover, because of the large number of atoms in the model, to correctly optimize the ZmPAO−inhibitor complexes obtained by docking, the following additional constraints had to be imposed: (i) the cofactor FAD and the oxygen atoms of the water molecules were frozen; (ii) the backbone of the entire protein was constrained with a force constant of 100 kJ/mol; (iii) the inhibitor and all the amino acid side chains were unconstrained during energy minimization to allow for reorientation and proper hydrogen-bonding geometries and van der Waals contacts.

In addition to docking calculations, GRID maps[36] were calculated for some atom or group probes to evaluate the regions of best interaction between the inhibitors and the macromolecule. Box dimensions were defined to accommodate all the residues constituting the binding site. The used probes were DRY (hydrophobic probe), C1= (sp^2 CH aromatic or vinyl), N1: (sp^3 NH with lone pair), N2: (sp^3 NH_2 with a lone pair), N3+ (sp^3 amine NH_3 cation), N1= (sp^2 amine NH cation), and N2= (sp^2 amine NH_2 cation). A value of 3 was used for the GRID keyword NPLA, which is the number of planes of grid points per Å and determines the resolution of the computation; the grid points were 0.333 Å apart. A value of 0 was used for the GRID keyword MOVE, thus allowing lone pairs and tautomeric hydrogen atoms to move in response to the probe. In order to achieve the points of the minimum of molecular interaction fields (MIFs), GRID calculations were performed for each probe separately and using the export GRIDKONT option. The kont files corresponding to each MIF were then processed by means of the minim and filmap programs (both implemented in the GRID package) that extract

all the points of the minimum of each MIF and retain only those falling under a user-defined cutoff. Threshold values of 0 kcal/mol were used for all three probes.

In a preliminary step, the reliability of the docking protocol was checked by simulations of the binding modes of **17** and **1** and a comparison of the modeled complexes with the available 3D structures derived by X-ray crystallography (1H82 and 1H83, respectively).[22] The double validation was necessary because the inhibitors in our hands could be classified into two different structural classes: (1) compounds with two guanidino moieties and with many (over 10) degrees of freedom, structurally similar to **17** of the 1H82 complex and (2) compounds with less than 10 torsionals, structurally similar to **1** found in the 1H83 complex. On this basis, it was crucial to verify that the computational protocol to be applied to inhibitors is also able to reproduce the binding modes of both **17** and **1**.

Structures of inhibitors were built using Maestro 3D-sketcher, minimized with OPLS_AA force field[42] using the PRCG algorithm (0.001 kJ/(Å·mol) convergence) and finally docked in the native protein. As a result, the experimental binding conformations of the reference compounds were successfully reproduced by applying the above-mentioned Autodock settings. In particular, for the crystallographic complex between ZmPAO and **17**, eight docking runs were performed. All the resulting conformers were merged and clustered (1.5 Å rms). The first ranked docked conformation belonging to the first cluster (25 conformers) was able to reproduce the X-ray conformation of **17** with a root-mean-square deviation (rmsd) of 0.08 Å on backbone atoms, 1.61 Å on heavy atoms, and 2.56 Å on all the atomic coordinates. Moreover, a comparison between calculated and experimental affinity showed that **17** had an estimated affinity of 33 nM versus an experimental value of 7.5 nM.

The validation step on 1,8-diaminooctane was performed in both the charged and uncharged form of the inhibitor, since, in the process of recognition of substrates and inhibitors by ZmPAO active site, the protonation state of the substrate and inhibitors within the tunnel has not yet been deterrmined unambiguously. In this case, for both the charged and uncharged forms of **1**, only one docking computation was carried out. When the inhibitor was docked in its protonated form, the best conformations belonging to the two most populated clusters (67 and 52 conformers, respectively) reproduced the two alternative crystallographic poses with 0.84 and 0.84 Å rmsd calculated on all the atomic coordinates. Simulation on the uncharged form showed that the best conformers were characterized by a marked increase of the rmsd values against the X-ray conformation of **1** oriented toward the narrow entrance of the catalytic tunnel, while the alternative orientation was not found by Autodock.

Although in several cases Autodock may be unable to correctly locate ligands within binding sites, results from simulations on **17** and a comparison with the corresponding X-ray structure led us to assume the docking protocol as a reliable procedure to be applied to the new inhibitors belonging to the class of iminoctadine derivatives. Moreover, Autodock calculations on *N*-prenylagmatine derivatives gave results, in terms of orientations and interactions of the ligands, in good agreement with those found by means of a pseudo Monte Carlo statistical conformational analysis previously performed on the same compounds.[25]

Molecular Dynamics (MD) Simulations. The complex between **19** and ZmPAO, as derived from docking simulations and energy minimization, was submitted to a MD protocol using MacroModel and the OPLS 2001[42] force field. GB/SA, with water parameters, was used to simulate the solvent. The starting structure was relaxed by performing 20 ps of MD at 310 K (equilibration phase). Next, the system was submitted to 1 ns of MD simulations (310 K), extracting a snapshot every 10.0 ps. Dynamics time step was set to 1.5 fs.

Supporting Information Available: Spectral and elemental analysis data of intermediates and final compounds; details of Dixon analysis; details of molecular modeling. This material is available free of charge via the Internet at http://pubs.acs.org.

References

(1) Wallace, H. M.; Fraser, A. V.; Hughes, A. A perspective of polyamine metabolism. *Biochem. J.* **2003**, *376*, 1–14.
(2) Seiler, N. Catabolism of polyamines. *Amino Acids* **2004**, *26*, 217–233.
(3) Cona, A.; Rea, G.; Angelini, R.; Federico, R.; Tavladoraki, P. Functions of amine oxidases in plant development and defence. *Trends Plant Sci.* **2006**, *11*, 80–88.
(4) Federico, R.; Alisi, C.; Forlani, F. Properties of the polyamine oxidase from the cell wall of maize seedlings. *Phytochemistry* **1989**, *28*, 45–46.
(5) Cervelli, M.; Cona, A.; Angelini, R.; Polticelli, F.; Federico, R.; Mariottini, P. A barley polyamine oxidase isoform with distinct structural features and subcellular localization. *Eur. J. Biochem.* **2001**, *268*, 3816–3830.
(6) Maiale, S. J.; Marina, M.; Sánchez, D. H.; Pieckenstain, F. L.; Ruiz, A. O. In vitro and in vivo inhibition of plant polyamine oxidase activity by polyamine analogues. *Phytochemistry* **2008**, *69*, 2552–2558.
(7) Wu, T.; Yankovskaya, V.; McIntire, W. S. Cloning, sequencing, and heterologous expression of the murine peroxisomal flavoprotein, N^1-acetylated polyamine oxidase. *J. Biol. Chem.* **2003**, *278*, 20514–20525.
(8) Vujcic, S.; Diegelman, P.; Bacchi, C. J.; Kramer, D. L.; Porter, C. W. Identification and characterization of a novel flavin-containing spermine oxidase of mammalian cell origin. *Biochem. J.* **2002**, *367*, 665–675.
(9) Landry, J.; Sternglanz, R. Yeast Fms1 is a FAD-utilizing polyamine oxidase. *Biochem. Biophys. Res. Commun.* **2003**, *303*, 771–776.
(10) Tavladoraki, P.; Rossi, M. N.; Saccuti, G.; Perez-Amador, M. A.; Polticelli, F.; Angelini, R.; Federico, R. Heterologous expression and biochemical characterization of a polyamine oxidase from Arabidopsis involved in polyamine back conversion. *Plant Physiol.* **2006**, *141*, 1519–1532.
(11) Moschou, P. N.; Sanmartin, M.; Andriopoulou, A. H.; Rojo, E.; Sanchez-Serrano, J. J.; Roubelakis-Angelakis, K. A. Bridging the gap between plant and mammalian polyamine catabolism: a novel peroxisomal polyamine oxidase responsible for a full back-conversion pathway in Arabidopsis. *Plant Physiol.* **2008**, *147*, 1845–1857.
(12) Seiler, N. Pharmacological aspects of cytotoxic polyamine analogs and derivatives for cancer therapy. *Pharmacol. Ther.* **2005**, *107*, 99–119.
(13) Ha, H. C.; Woster, P. M.; Yage, J. D.; Casero, R. A. The role of polyamine catabolism in polyamine analogue-induced programmed cell death. *Proc. Natl. Acad. Sci. U.S.A.* **1997**, *94*, 11557–11562.
(14) Hu, R. H.; Pegg, A. E. Rapid induction of apoptosis by deregulated uptake of polyamine analogues. *Biochem. J.* **1997**, *328*, 307–316.
(15) Devereux, W.; Wang, Y.; Stewart, T. M.; Hacker, A.; Smith, R.; Frydmann, B.; Valasinas, A. L.; Reddy, V. K.; Marton, L. J.; Ward, T. D.; Woster, P. M.; Casero, R. A. Induction of the PAOh1/SMO polyamine oxidase by polyamine analogues in human lung carcinoma cells. *Cancer Chemother. Pharmacol.* **2003**, *52*, 383–390.
(16) Chaturvedi, R.; Cheng, Y.; Asim, M.; Bussière, F. I.; Xu, H.; Gobert, A. P.; Hacker, A.; Casero, R. A.Jr.; Wilson, K. T. Induction of polyamine oxidase 1 by *Helicobacter pylori* causes macrophage apoptosis by hydrogen peroxide release and mitochondrial membrane depolarization. *J. Biol. Chem.* **2004**, *279*, 40161–40173.
(17) Xu, H.; Chaturvedi, R.; Cheng, Y.; Bussière, F. I.; Asim, M.; Yao, M. D.; Potosky, D.; Meltzer, S. J.; Rhee, J. G.; Kim, S. S.; Moss, S. F.; Hacker, A.; Wang, Y.; Casero, R. A.Jr.; Wilson, K. T. Spermine oxidation induced by *Helicobacter pylori* results in apoptosis and DNA damage: implications for gastric carcinogenesis. *Cancer Res.* **2004**, *64*, 8521–8525.
(18) Babbar, N.; Casero, R. A.Jr. Tumor necrosis factor-α increases reactive oxygen species by inducing spermine oxidase in human lung epithelial cells: a potential mechanism for inflammation-induced carcinogenesis. *Cancer Res.* **2006**, *66*, 11125–11130.
(19) Yoda, H.; Hiroi, Y.; Sano, H. Polyamine oxidase is one of the key elements for oxidative burst to induce programmed cell death in tobacco cultured cells. *Plant Physiol.* **2006**, *142*, 193–206.
(20) Wood, P. L.; Khan, M. A.; Kulow, S. R.; Mahmood, S. A.; Moskal, J. R. Neurotoxocity of reactive aldehydes: the concept

of "aldehyde load" as demonstrated by neuroprotection with hydroxylamines. *Brain Res*. **2006**, *1095*, 190–199.
(21) Binda, C.; Coda, A.; Angelini, R.; Federico, R.; Ascenzi, P.; Mattevi, A. A 30 Å long U-shaped catalytic tunnel in the crystal structure of polyamine oxidase. *Structure* **1999**, *7*, 265–276.
(22) Binda, C.; Angelini, R.; Federico, R.; Ascenzi, P.; Mattevi, A. Structural bases for inhibition binding and catalysis in polyamine oxidase. *Biochemistry* **2001**, *40*, 2766–2776.
(23) Cervelli, M.; Polticelli, F.; Federico, R.; Mariottini, P. Heterologous expression and characterization of mouse spermine oxidase. *J. Biol. Chem*. **2003**, *278*, 5271–5276.
(24) Bianchi, M.; Polticelli, F.; Ascenzi, P.; Botta, M.; Federico, R.; Mariottini, P.; Cona, A. Inhibition of polyamine and spermine oxidases by polyamine analogues. *FEBS J*. **2006**, *273*, 1115–1123.
(25) Cona, A.; Manetti, F.; Leone, R.; Corelli, F.; Tavladoraki, P.; Polticelli, F.; Botta, M. Molecular basis for the binding of competitive inhibitors of maize polyamine oxidase. *Biochemistry* **2004**, *43*, 3426–3435.
(26) Stránská, J.; Šebela, M.; Tarkowski, P.; Řehulka, P.; Chmelík, J.; Popa, I.; Peč, P. Inhibition of plant amine oxidase by a novel series of diamine derivatives. *Biochimie* **2007**, *89*, 135–144.
(27) Federico, R.; Leone, L.; Botta, M.; Binda, C.; Angelini, R.; Venturini, G.; Ascenzi, P. Inhibitor of pig liver and *Zea mays* L. polyamine oxidase: a comparative study. *J. Enzyme Inhib*. **2001**, *13*, 465–471.
(28) Corelli, F.; Federico, R.; Cona, A.; Venturini, G.; Schenone, S.; Botta, M. Solution and solid-phase synthesis of aminoalkylguanidines inhibiting polyamine oxidase and nitric oxide synthase. *Med. Chem. Res*. **2002**, *11*, 309–321.
(29) Dreassi, E.; Zizzari, A. T.; D'Arezzo, S.; Visca, P.; Botta, M. Analysis of guazatine mixture by LC and LC−MS and antimycotic activity determination of principal components. *J. Pharm. Biomed. Anal*. **2007**, *43*, 1499–1506.
(30) Artiss, J. D.; Entwistle, W. M. The application of a sensitive uricase−peroxidase couple reaction to a centrifugal fast analyser for the determination of uric acid. *Clin. Chim. Acta* **1981**, *116*, 301–309.
(31) Dixon, M. The determination of enzyme inhibitor constants. *Biochem. J*. **1953**, *55*, 170–171.
(32) QikProp, version 3.0; Schrodinger, LLC: New York, 2007.
(33) Artursson, P.; Karlsson, J. Correlation between oral drug absorption in humans and apparent drug permeability coefficients in human intestinal epithelial (Caco-2) cells. *Biochem. Biophys. Res. Commun*. **1991**, *175*, 880–885.
(34) Casero, R. A.Jr.; Mank, A. R.; Xiao, L.; Smith, J.; Bergeron, R. J.; Celano, P. Steady-state messenger RNA and activity correlates with sensitivity to N1,N12-bis(ethyl)spermine in human cell lines representing the major forms of lung cancer. *Cancer Res*. **1992**, *52*, 5359–5363.
(35) Huang, Q.; Liu, Q.; Hao, Q. Crystal structures of Fms1 and its complex with spermine reveal substrate specificity. *J. Mol. Biol*. **2005**, *348*, 951–959.
(36) GRID, version 22; Molecular Discovery, Ltd.: Marsh Road, Pinner, Middlesex, U.K.
(37) Mosmann, T. Rapid colorimetric assay for cellular growth and survival: application to proliferation and cytotoxicity assays. *J. Immunol. Methods* **1983**, *65*, 55–63.
(38) Morris, G. M.; Goodsell, D. S.; Halliday, R. S.; Huey, R.; Hart, W. E.; Belew, R. K.; Olson, A. J. Automated docking using a Lamarckian genetic algorithm and an empirical binding free energy function. *J. Comput. Chem*. **1998**, *19*, 1639–1662.
(39) Mohamadi, F.; Richards, N. G. J.; Guida, W. C.; Liskamp, R.; Lipton, M.; Caufield, C.; Chang, G.; Hendrickson, T.; Still, W. C. An integrated software system for modeling organic and bioorganic molecules using molecular mechanics. *J. Comput. Chem*. **1990**, *11*, 440–467.
(40) Maestro, version 7.5; Schroedinger: New York, 2006.
(41) Dewar, M. J. S.; Zoebisch, E. G.; Healy, E. F.; Stewart, J. J. P. AM1: a new general purpose quantum mechanical molecular model. *J. Am. Chem. Soc*. **1985**, *107*, 3902–3909.
(42) Jorgensen, W. L.; Maxwell, D. S.; Tirado-Rives, J. Development and testing of the OPLS all-atom force field on conformational energetics and properties of organic liquids. *J. Am. Chem. Soc*. **1996**, *118*, 11225–11236.